Asymmetrical Fault Ride Through as Ancillary Service by Constant Power Loads in Grid-Connected Wind Farm

Nadeem Jelani, *Member, IEEE*, and Marta Molinas, *Member, IEEE*

***Abstract*—The introduction of distributed generation (DG) into low voltage (LV) systems demands that the generation system remain grid connected during voltage sags to ensure the operational stability. The DG consisting of fixed speed squirrel cage induction generator (SCIG)-based wind turbines is unable to provide reactive power control and needs a dedicated compensating device. Under asymmetrical grid faults the negative sequence flux circulation in the airgap introduces the torque oscillations that lead to the reduction of lifetime of the generation system. This paper proposes the use of distributed constant power loads (CPLs) for asymmetrical fault ride through (FRT) instead of using a centralized STATCOM. It has also been observed that the compensation of negative sequence voltage improves the performance of SCIG by eliminating the torque ripples. The compensation of positive sequence voltage avoids a possible voltage collapse at the LV distribution level and improves the reliability and stability of the wind farm. Centralized compensation of the asymmetrical grid fault by a STATCOM is compared with the distributed compensation by CPLs. The results suggest that each individual CPL injects lower current for maximum FRT enhancement compared to a dedicated STATCOM.**

***Index Terms*—Constant power loads (CPLs), distributed energy systems, fault ride through (FRT), power electronics (PEs), reactive power control, voltage source converters (VSCs).**

I. Introduction

DUE to the environment advantages and being close to the point of power utilization the use of renewable energy resources is rapidly growing at the distribution level. Among them, photovoltaic and wind turbines are gaining increasing attention [1]. Power generation from wind energy and its integration to the local distribution grid is relatively newer approach [2]. In the last decade, the technological developments have made it possible to change the generator types used for wind farm from fixed speed to variable speed concept. However, squirrel cage induction generator (SCIG)-based wind farms represent a considerable 30% of the installed wind power in Europe [3] and enhancing their fault ride through (FRT) capability is indispensable in order to increase the power system stability and reliability [4], [5]. Additionally, for microhydroapplications, SCIG is still the cost effective and reliable power generation source.

To maintain the stability of the utility grid, grid operators have specified the requirements for the integration of DERs. For wind power plants, the grid connection requirements demand FRT capability and reactive current injection in order to maintain the stability of the power system [6]–[10]. In UK, FRT capability requirements demand that terminal voltage of the wind farm should not be less than 15% of the nominal voltage during the fault and it must be restored to 90% within 0.5 s. Grid codes in Denmark set the minimum voltage level during the fault to 25% of the nominal voltage and it should be restored to 75% within 0.75 s [6]–[8]. These grid codes requirements are independent of the type of compensators and can be achieved by using either active or passive compensators. In the case of SCIG-based wind farms, the absence of any power electronic (PE) compensating device does not allow FRT enhancement and reactive current injection to fulfill the grid code requirements.

Different methods have been investigated to fulfill the grid code requirements and enhance the FRT capability of a wind farm. These include the use of doubly fed induction generator (DFIG)-based wind farms for variable speed applications and a centralized STATCOM for fixed speed applications [11]–[19]. It has been observed that DFIG experiences inherent difficulties to ride through grid faults due to the high voltage induced in the rotor circuit. Many practical strategies of STATCOM reactive power control under asymmetrical grid faults and load unbalances have been discussed in [5] and [17] and proved to be very effective. However, the installation of a dedicated switching compensator or a STATCOM is not very cost effective. The rapidly changing modern power infrastructure can utilize some of its installed resources for the services that were earlier provided by the dedicated devices.

PE load interface, when tightly regulated, draws a constant active power from the utility and behaves as a constant power load (CPL). It is adaptive to the fluctuations in the grid voltage at its terminal and always keeps the input power constant [20]–[29]. The number of this kind of load has been rapidly growing and will continue to increase in the near future. Battery charger for electric vehicles, motor drives and large rectifiers for DC loads are few examples of CPLs. The use of single CPL for FRT enhancement has been discussed in [29] as a starting point using a basic distribution system model. The study, however, provides

Manuscript received October 8, 2013; revised March 12, 2014; accepted April 17, 2014. Date of publication April 29, 2014; date of current version October 15, 2014. This work was supported in part by the Higher Education Commission of Pakistan. Recommended for publication by Associate Editor B. Lehman.

The authors are with the Department of Electric Power Engineering, Norwegian University of Science and Technology, Trondheim 7050, Norway (e-mail: nadeem.jelani@elkraft.ntnu.no; marta.molinas@elkraft.ntnu.no).

Color versions of one or more of the figures in this paper are available online at http://ieeexplore.ieee.org.

Digital Object Identifier 10.1109/TPEL.2014.2320949

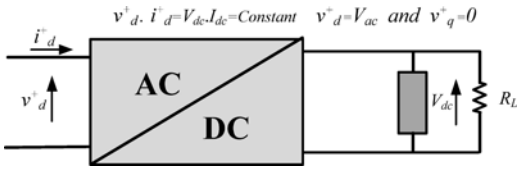

Fig. 1. Basic model of a CPL.

no comparison of the current rating of the PE devices acting as CPLs with the existing STATCOM solution. The modern distribution systems have many CPLs distributed across the network and the proper utilization of these resources for ancillary grid services is more practical and beneficial to improve the efficiency and performance of the entire power system compared to the use of a single CPL reported in [29].

This paper proposes the application of tightly regulated PE load interfaces or CPLs, connected to fixed speed SCIG-based wind farm for FRT enhancement under asymmetrical grid faults. For variable speed applications, CPLs can help to reduce the current rating of the generation side converters on each wind turbine by sharing some of the ancillary services. In addition to the typical positive sequence reactive current injection, the proposed method suggests a negative sequence active and reactive current injection during the FRT operation to mitigate the voltage unbalances without exceeding the peak current limit of the PE load interface. A comparison between the distributed compensation of active and reactive power by CPLs and the centralized compensation by a STATCOM indicates a lower per unit current rating for each distributed PE device compared to the centralized compensation solution offered by STATCOM.

II. CPL and Negative Resistance

CPL is usually an active rectifier such as three-phase full-bridge inverter with IGBTs or other similar switching semiconductor devices. Three-phase diode and tyristor front end rectifiers can be used as CPL but they do not provide much control flexibility. An active rectifier provides more flexibility in operation, power factor controllability and reduced THD. A well-known application of an active rectifier is a voltage source converter (VSC) as it is naturally suited for controlling active and reactive current in a decoupled manner using vector control principles [30]. In this way, the inverter can control the direct current component absorbed toward the load independently of the control of reactive current, which can be injected toward the grid, thus supporting the stability of the power system under abnormal grid voltage conditions. Fig. 1 illustrates the simplified model of a CPL.

Like many other nonlinear loads the resistance of the CPL depends on the applied voltage at its terminals. Many of the home appliances are loads with ac/dc converters inside, feeding an internal part that works on a constant dc voltage [28]–[31]. The control system of these ac/dc converters controls the direct voltage $V_{\rm dc}$ such that it becomes independent of the applied grid voltage v_d^+. This means that the ac power is independent of the value of grid voltage. A lower ac side voltage from the rated value results in a drop in dc-link voltage. However, the increase in ac side current neutralizes the drop in dc-link voltage which remains constant under all the conditions. The load resistance R_L translates the active power demand by the load and can be varied accordingly adjusting the load current. Under symmetrical grid voltage sags with no negative sequence voltage present in the system, the operation of the internal controller demands the VSC to draw more/less grid current to maintain a constant active power at the converter input, such that

$$v_d^+ = \frac{P_{\rm in}}{i_d^+} \tag{1}$$

where $P_{\rm in}$ is the constant input active power and i_d^+ and v_d^+ are the positive sequence active components of the ac side current and voltage respectively. Since the input active power to the converter remains constant in a wide range of operating conditions, provided that the controller works properly, the *vi* characteristic of the CPL is investigated by considering the incremental input resistance $R_{\rm CPL}$ [32]. This value is given by the ratio of small-signal changes in input positive sequence voltage over small-signal positive sequence input current

$$R_{\rm CPL} \approx \frac{\Delta v_d^+}{\Delta i_d^+}. \tag{2}$$

Differentiating (1) with respect to the positive sequence current yields negative input resistance

$$\frac{dv_d^+}{di_d^+} = -\left|\frac{P_{\rm in}}{i_d^{+2}}\right| = -\left|\frac{v_d^{+2}}{P_{\rm in}}\right| = -R_{\rm CPL}. \tag{3}$$

$R_{\rm CPL}$ represents the negative resistance seen from the ac side. When the negative incremental resistance is combined with the converter filters that are placed to avoid the effects of the high frequency switching, negatively damped oscillations may develop. The stability of the converter as well as the system to which it is part of depends on the proper damping of the negative incremental resistance due to CPL characteristic. For distributed ac and hybrid ac/dc systems with CPLs, the very first design-oriented stability criteria have been developed in [20] and [21]. In this paper, the stability criteria for a CPL to choose proper components of a single-stage *LC* filter based on the Brayton–Moser mixed potential theory has been derived. Moreover, ac stability criterion has been introduced based on the generalized Nyquist criterion and reference frame theory. The research has been further put forward in a more recent work reported in [22], [23]. A generalized state-space averaging method to investigate the negative impedance instability in hybrid ac/dc distribution systems has been reported in [24] and [25]. A stable region for a typical system has been presented. Some recommendations have been suggested to avoid negative impedance instability when designing ac power systems. The destabilizing effects of the negative resistance can also be minimized by enabling the CPL to inject the positive sequence reactive current i_q^+ as suggested in the subsequent sections. This reactive injection leads to a small increase in positive sequence voltage at the CPL terminal and the active component of the positive sequence current decreases to keep the input power constant.

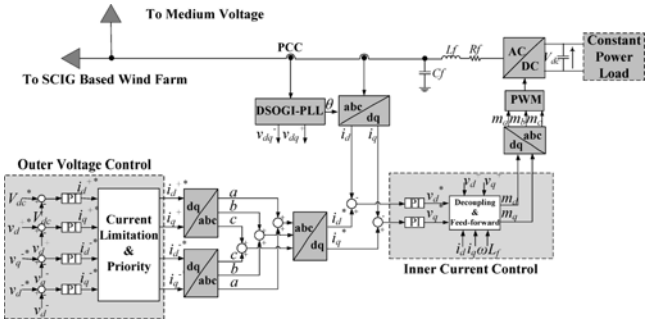

Fig. 2. CPL control structure with independent control of positive and negative sequence voltages at PCC.

III. Control Structure for Asymmetrical Grid Voltage Compensation

The implemented CPL control is based on vector control principle in rotating synchronous reference frame (SRF). The overall control structure is presented in Fig. 2. An independent control of positive and negative sequence voltages demands the precise sequence extraction to be incorporated into the control structure. To achieve the FRT enhancement, the CPL control algorithm injects the negative sequence active current and both the positive and the negative sequence reactive current. Four PI regulators have been added in the outer voltage control while inner current control includes two more PI regulators. Positive sequence reactive current i_q^+ compensates the positive sequence active voltage drop v_d^+ while the negative sequence reactive current i_q^- compensates for the negative sequence active voltage drop v_d^-. Negative sequence active current i_d^- is injected by CPL to compensate the negative sequence reactive voltage drop v_q^-. CPL also absorbs the positive sequence active current i_d^+ to meet the load power requirements and maintain the dc-link voltage.

The outer control loops are designed to control the dc-link voltage and the positive and negative sequence of the voltage at the point of common coupling (PCC). The basic CPL control structure is based on the outer dc-link voltage controller and the inner current controllers. However, the ancillary FRT enhancement demands the incorporation of positive and negative sequence voltage controllers in the outer control loop. For this purpose, a precise sequence separation of the PCC voltage into positive and negative sequence components is required. A phase lock loop (PLL) based on dual second-order generalized integrator (DSOGI) has been employed for this purpose. Using the DSOGI–PLL sequence separation scheme, the positive and negative sequence of the voltage appear as dc values in SRF and can be easily controlled by using PI controller. The current limitation and priority block presented in Fig. 2 adjusts the level of positive and negative sequence active and reactive currents so that a predefined ampere constraint (1.0 p.u.) of the CPL is not exceeded; thus, the risk of overcurrent tripping of the CPL can be avoided. The priority has been given to the positive sequence reactive current i_q^+ to compensate the positive sequence voltage, thereby making sure the maximum FRT and stability enhancement of the SCIG-based wind farm. The remaining current capacity of the CPL is used to compensate the negative sequence voltage in order to reduce the torque pulsations during the unbalanced grid fault.

A. Selection of Controller Parameters

The optimal controller operation requires lowest possible overshoot and fast response which can be achieved by keeping the cutoff frequency higher. To obtain the described objectives, modulus optimum and symmetrical optimum tuning methods have been implemented to select the parameters for inner current controller and outer dc-link voltage controller, respectively [33].

Modulus optimum technique is used for the plants with low-order transfer functions and makes the cutoff frequency as high as possible. When the system has one dominant and another minor pole in the transfer function, the integral time constant of the PI controller is selected to cancel out the dominant pole. The open-loop transfer function of the inner current controllers is the combination of transfer functions of PI regulator, PWM converter and the system as reported in [33] and can be represented as

$$H_{C,OL}(s) = K_{pc} \cdot \left(\frac{1+T_{ic}s}{T_{ic}\cdot s}\right) \cdot \left(\frac{1}{1+T_a\cdot s}\right) \cdot \left(\frac{1}{Rf\cdot(1+s\cdot\tau)}\right) \tag{4}$$

where the subscript "c" represents the current controller. K_{pc} is the proportional gain and T_{ic} is the integral time constant, T_a is the average delay of the PWM converter, R_f is the filter resistance, and τ is the time constant of the distribution line.

The zero of the PI controller is cancelled out by defining $T_{ic} = \tau$. The open-loop transfer function hence reduces to

$$H_{C,OL}(s) = \frac{K_{pc}}{\tau\cdot R_f}\cdot\frac{1}{s\cdot(1+T_a\cdot s)}. \tag{5}$$

The close-loop transfer function can be presented as

$$H_{C,CL}(s) = \frac{K_{pc}}{\tau\cdot R_f\cdot T_a\cdot s^2+\tau\cdot Rf\cdot s+1}. \tag{6}$$

The controller gain is calculated from the unity gain condition at cutoff frequency such that

$$|H_{C,CL}(j\omega)| = \left|\frac{K_{pc}}{\tau\cdot R_f\cdot T_a\cdot(j\omega)^2+\tau\cdot R_f\cdot(j\omega)+1}\right| = 1. \tag{7}$$

The evaluation of (7) provides the value of inner current controller proportional gain K_{pc}, such that

$$K_{pc} = \frac{\tau R_f}{2T_a}. \tag{8}$$

Modulus optimum criterion is not a good choice in a case where one pole of the open-loop transfer function is close to or at the origin. Instead, symmetrical optimum tuning technique is used to select the PI controller parameters [33]. The main advantage of the tuning schemes is that it maximizes the phase margin and optimizes the control system behavior with respect to disturbance input.

TABLE I
PARAMETERS OF THE INNER CURRENT AND OUTER DC-LINK VOLTAGE CONTROLLER

Parameter	Value
Base frequency f	50 Hz
Switching frequency f_{sw}	5 kHz
Average time delay T_a	100 µs
Integral time constant T_{ic}	0.016 s
Proportional gain K_{pc}	0.8
Integral gain K_{ic}	50
Equivalent time delay T_{eq}	200 µs
Integral time constant T_{iv}	0.0018 s
Capacitor time constant T_c	0.0024 s
Proportional gain K_{pv}	4
Integral gain K_{iv}	2222.22
Steady state voltage ratio K	1

The equivalent open-loop transfer function of the outer dc-link voltage controller can be represented by the combination of transfer functions of PI regulators, inner current controller and system as presented in [33], such that

$$H_{V,OL}(s) = K_{pv} \cdot \left(\frac{1 + T_{iv} \cdot s}{T_{iv} \cdot s}\right) \cdot \left(\frac{1}{1 + T_{eq} \cdot s}\right) \cdot \left(\frac{v_d^+}{V_{dc}} \cdot \frac{\omega b \cdot C}{s}\right) \quad (9)$$

where the subscript ''v" represents the voltage controller. K_{pv} is the proportional gain and T_{iv} is the integral time constant, T_{eq} is the average delay of the current controller, C represents the dc-link capacitor.

Equation (9) is simplified by defining the $T_c = 1/\omega_b.C$ and $K = v_d^+/V_{\rm dc}$, such that

$$H_{V,OL}(s) = K_{pv} \cdot \left(\frac{1 + T_{iv} \cdot s}{T_{iv} \cdot s}\right) \cdot \left(\frac{K}{1 + T_{eq} \cdot s}\right) \cdot \left(\frac{1}{s \cdot Tc}\right). \quad (10)$$

According to the tuning criteria based on Nyquist stability, the parameters of the outer dc-link voltage controller are found as

$$K_{pv} = \frac{T_c}{a \cdot K \cdot T_{eq}} \text{ and } T_{iv} = a^2 T_{eq}$$
$$\text{where,} \quad a = \sqrt{\frac{1 + \sin\Phi_M}{1 - \sin\Phi_M}}$$
$$\text{Phase Margin,} \quad \Phi_M = \tan^{-1}\sqrt{\frac{T_{iv}}{T_{eq}}} - \tan^{-1}\sqrt{\frac{T_{eq}}{T_{iv}}} \quad (11)$$

where a is a constant number and its recommended value is between 2 and 4 [33]. Using (8) and (11), the parameters of inner and outer controllers are calculated and summarized in Table I. The parameters of the outer positive and negative sequence voltage controllers are found on the trial and error basis as their role is to provide the ancillary services and they are not the part of basic CPL control structure comprising of dc-link voltage and inner current controllers.

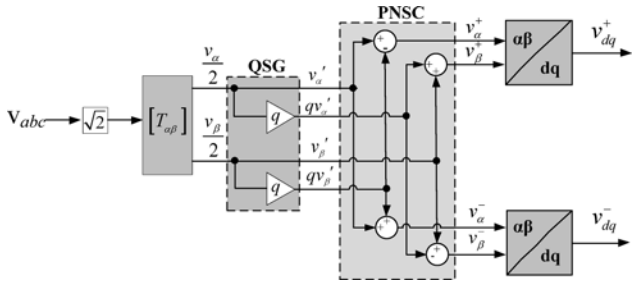

Fig. 3. Positive and negative sequence calculation in SRF.

B. Sequence Separation

The positive and negative sequence detection technique named as DSOGI–PLL translates the three-phase voltage from the *abc* to stationary $\alpha\beta$ reference frames [34]–[38]. DSOGI-based quadrature signals generator (QSG) is employed for filtering and obtaining the 90° shifted versions from the $\alpha\beta$ voltages. The QSG output signals act as inputs to the positive and negative sequence calculator (PNSC) [34]–[37]. The positive and negative sequence $\alpha\beta$ voltages are then transformed to the rotating SRF, such that

$$v_{dq}^+ = \left[T_{dq}^+\right] v_{\alpha\beta}^+ = \begin{bmatrix} \cos\theta & \sin\theta \\ -\sin\theta & \cos\theta \end{bmatrix} v_{\alpha\beta}^+$$
$$v_{dq}^- = \left[T_{dq}^-\right] v_{\alpha\beta}^- = \begin{bmatrix} \cos\theta & -\sin\theta \\ \sin\theta & \cos\theta \end{bmatrix} v_{\alpha\beta}^- \quad (12)$$

where v_{dq}^+ and v_{dq}^- are the instantaneous positive and negative sequence voltage components in SRF while $v_{\alpha\beta}^+$ and $v_{\alpha\beta}^-$ represents the positive and negative sequence voltage components in stationary $\alpha\beta$ reference frame. Fig. 3 represents the QSG and PNSC used for the extraction of positive and negative sequence voltage in SRF.

IV. POWER SYSTEM STRUCTURE WITH DISTRIBUTED CPLS

The investigated power system is shown in Fig. 4. It consists of a 3 MW fixed speed SCIG-based wind farm connected directly to the medium voltage grid. Several CPLs are connected to the low voltage (LV) distribution bus. It has been assumed that the distribution level is entirely dominated by the consumers with PE interfaces at the front end. The main grid is a three-phase ac source with internal impedance. An aggregate model of the wind farm is used so that the sum of the turbines is modeled as one generator using the standard T-equivalent circuit. $\rm CPL_1$ will be occasionally replaced with a centralized STATCOM. The transformer is rated for wind farm. The grid fault occurs at the medium voltage bus. The inductance L_g of the transmission line is assumed to be 1 mH per kilometer. The inductance L_p and resistance R_p of the distribution line is assumed to be 1 mH and 0.1 Ω per kilometer, respectively [39]. All the power system parameters are presented in Table II. The power system has been modeled in $\rm PSCAD/EMTDC$ software.

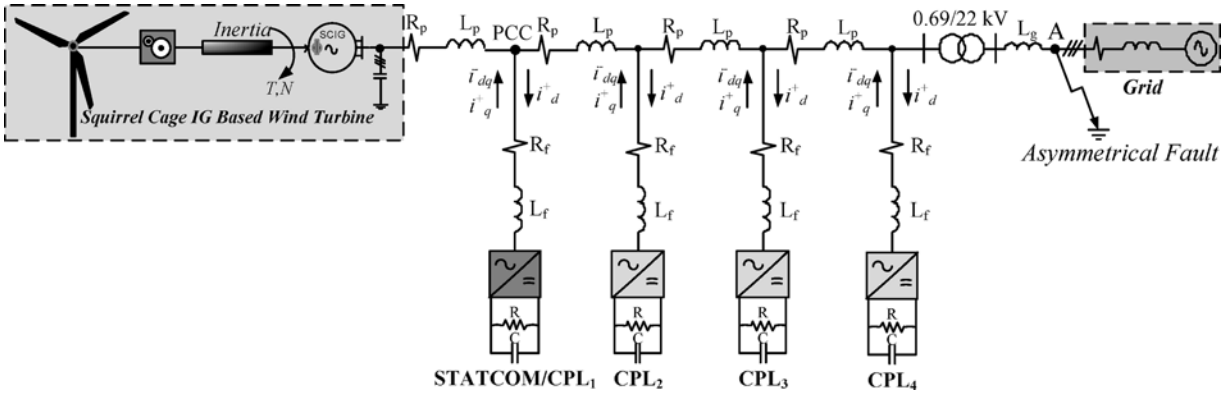

Fig. 4. Structure of the investigated system with SCIG-based wind farm and distributed CPLs.

TABLE II
WIND FARM, CPL, GRID, AND LINES PARAMETERS

Wind Farm	
Base Apparent Power	3.36 MVA
Rated Active Power	3 MW
Rated Voltage (line to line)	690 V
Stator resistance	0.0092 pu
Stator leakage inductance	0.1580 pu
Mutual inductance	3.87 pu
Rotor mutual inductance	0.0651 pu
Polar moment of inertia	0.5 s
Mechanical damping	0.008 pu
Constant Power Load (Individual Device)	
Rated Power	3 MVA
Rated Voltage (line to line)	690 V
Filter Inductance L_f	0.21 pu
Filter Resistance R_f	0.042 pu
DC Link Voltage V_{dc}	1126 V
Grid and Lines	
Rated Voltage (line to line)	22 kV
Rated Frequency	50 Hz
Resistance	3.52 pu
Inductance	11 pu
Transmission Line Inductance	66.5 pu
Distribution Line Inductance L_P	0.11 pu
Distribution Line Resistance R_P	0.0353 pu

A. Operation of SCIG Under Grid Voltage Sag

Apart from many advantages such as low price, robust design, overload handling and little maintenance, the biggest disadvantage of SCIG is the uncontrollable reactive power consumption. The compensation for the reactive power consumption needs shunt capacitor banks at no-load [40], [41]. SCIG easily becomes unstable under LV conditions as low terminal voltage increases the rotor slip and consumption of reactive power, thereby, further lowering the voltage which leads to disconnection of the turbine.

The torque T^+ of the induction generator has a quadratic dependence on the positive sequence stator voltage magnitude [41] and can be represented by

$$T^+(s) = 3 \cdot \frac{p}{2} \cdot \frac{R_r}{s\omega_s} \cdot \frac{V_s^{+2}}{(R_s + R_r/s)^2 + j(X_s + X_r)^2} \quad (13)$$

where R_s, R_r, X_s, and X_r are the stator and rotor resistance and impedance parameters of the SCIG equivalent circuit, p is the number of pole pairs, s is the slip and ω_s is the grid frequency. For a smaller voltage dip, the SCIG may regain a stable operating point, but for a deep voltage dip the SCIG loses its torque control and may have to be disconnected from the grid due to over speed or a voltage collapse may happen in the network due to high reactive power consumption.

Under the unbalance voltage conditions, the stator currents become unbalanced too and even a small amount of negative sequence voltage V_s^- results in a very high negative sequence current I_s^- [41], such that

$$I_s^- = \frac{V_s^-}{\omega_s \cdot \sigma \cdot L_s \cdot I_{s,N}} \quad (14)$$

where L_s is the stator inductance, $I_{s,N}$ is the rated stator current and σ is the leakage factor. Average torque is not much affected by the negative sequence current; however, it causes the torque ripples of double grid frequency. The magnitude of the positive sequence torque and negative sequence torque T^- can be represented by Anaya-Lara *et al.* [41]

$$\begin{aligned} T^+ &\approx 3 \cdot \frac{p}{2\omega_s} \cdot V_s^+ \cdot I_s^+ \\ T^- &\approx 3 \cdot \frac{p}{2\omega_s} \cdot V_s^+ \cdot I_s^-. \end{aligned} \quad (15)$$

Due to the decreased positive sequence voltage magnitude, the average torque is reduced, leading to the acceleration of the generator. The additional torque oscillations of the double-grid frequency result in the heating of the stator windings and reduced lifetime of the turbine drive train. The average torque and the torque ripples can only be controlled independently if the CPLs are able to control the positive and negative sequence voltages.

V. RESULTS FOR UNBALANCED FRT ENHANCEMENT

In this section, a detailed simulation study has been carried out to investigate the FRT capability of the installed distributed CPLs at the distribution level supplied by SCIG-based wind farm. The power system as presented in Fig. 4 has been considered and the STATCOM is replaced with CPL_1 for this analysis. All the four CPLs are controlled to provide the FRT services and are equipped with both the voltage and current controllers utilizing the same parameters as discussed in Section III. Each

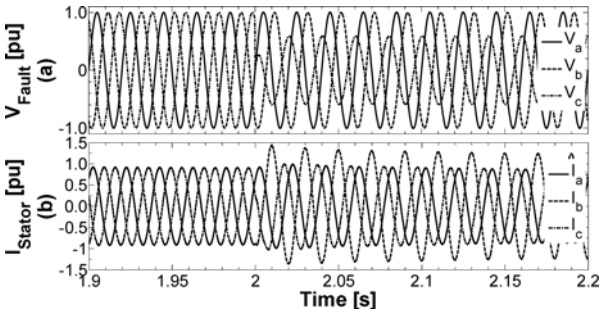

Fig. 5. (a) Three-phase voltages at the fault location (b) SCIG stator currents.

CPL starts consuming 450 kW power from the wind farm at time $t = 1$ s. An asymmetrical fault [single-phase amplitude falls to 60% as shown in Fig. 5(a)] is simulated at the medium voltage bus as presented in Fig. 4 at time $t = 2$ s for a duration of 1 s. The unbalanced grid fault leads to highly unbalanced currents in the stator of the SCIG as shown in Fig. 5(b).

In the presence of positive and negative sequence components in both voltage and current, the total apparent power can be expressed as

$$\begin{aligned} S = VI^* &= (V^+ + V^-)(I^+ + I^-)^* \\ &= (v_d^+ + jv_q^+ + v_d^- + jv_q^-)(i_d^+ + ji_q^+ + i_d^- + ji_q^-)^*. \end{aligned} \tag{16}$$

Further expansion of (16) results in real and reactive powers, such that

$$\begin{aligned} P_{CPL} &= v_d^+ i_d^+ + v_d^- i_d^- + v_q^- i_q^- + v_d^+ i_d^- + v_d^- i_d^+ + v_q^- i_q^+ \\ Q_{CPL} &= v_d^+ i_q^+ + v_d^- i_q^- - v_q^- i_d^- + v_d^- i_q^+ - v_q^- i_d^+ - v_d^+ i_q^- \end{aligned} \tag{17}$$

where P_{CPL} and Q_{CPL} are the CPL active and reactive powers.

A. CPLs Without Voltage Control

At the very start of the simulation analysis, the ac voltage control has been disabled for all the CPLs and the results are presented in Fig. 6. DC-link voltage control, however, remains active. The unbalanced fault leads to a negative sequence voltage as depicted in Fig. 6(a). In order to simplify the analysis, the positive and negative sequence voltages are shown as the quadratic sum of corresponding active and reactive components such that

$$\begin{aligned} v_{dq}^+ &= \sqrt{(v_d^+)^2 + (v_q^+)^2} \\ v_{dq}^- &= \sqrt{(v_d^-)^2 + (v_q^-)^2} \end{aligned} \tag{18}$$

where $v_q^+ = 0$, as d-axis is always synchronized with the grid voltage vector. The compensation current has also been presented by the corresponding quadratic sums.

The negative sequence voltage causes negative sequence flux circulation in the air gap and, therefore, results in torque ripples of the system during the fault. The torque oscillations put a huge stress on the mechanical part. The drop in the positive sequence voltage leads to a decrease in the torque and the speed of the rotor keeps on increasing as shown in Fig. 6(c). The severity of the fault drives the system to a mechanical unstable

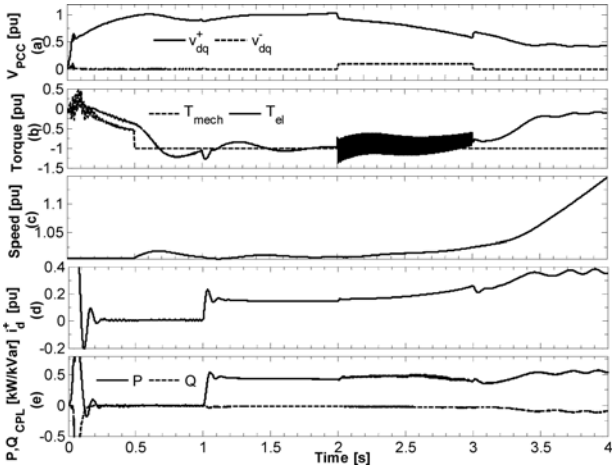

Fig. 6. Simulation results for CPLs without voltage control: (a) positive and negative sequence voltages at PCC, (b) SCIG torque, (c) SCIG speed, (d) active component of CPL_1 current representing the load power, and (e) CPL_1 powers.

point and a complete voltage collapse occurs due to high reactive power consumption by the SCIG as illustrated in Fig. 6(a). SCIG cannot return to the rated operating point after the fault. Fig. 6(d) shows the component of positive sequence active current i_d^+ corresponding to the CPL_1 active power input. The presence of only positive sequence active current i_d^+ reduces the power relationship presented by (17), such that

$$\begin{aligned} P_{\mathrm{CPL}} &= v_d^+ i_d^+ + v_d^- i_d^+ \\ Q_{\mathrm{CPL}} &= -v_q^- i_d^+ \,. \end{aligned} \tag{19}$$

During the fault, CPLs try to keep the active power constant by increasing the positive sequence active current; however, due to the complete voltage collapse the CPL control does not remain very effective and the input power cannot be kept constant as shown in Fig. 6(e). A very small amount of active and reactive power oscillations of double grid frequency are also present due to the interaction of negative sequence voltages with positive sequence input current as indicated by (19).

B. CPLs With Positive Sequence Voltage Control

In this case, the simulations are repeated for the same fault condition and CPLs are controlled to compensate for the positive sequence voltage only. The negative sequence voltage control remains inactive. The results have been presented in Fig. 7. The CPLs are able to compensate the positive sequence voltage at PCC by injecting the component of positive sequence reactive current i_q^+ as shown in Fig. 7(d). This avoids an increase in the positive sequence active current during the fault as is observed in the previous case. Due to the positive sequence voltage compensation, the speed of the rotor does not increase, confirming a stable operating point for the system unlike the previous case. Each CPL also consumes positive sequence active current component. The active and reactive powers associated with each CPL are shown in Fig. 7(e) for CPL_1 only and are represented

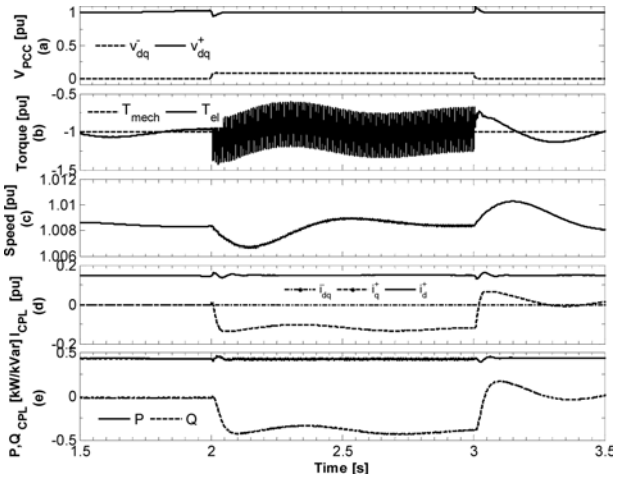

Fig. 7. Simulation results for positive sequence voltage control: (a) PCC voltages, (b) SCIG torque, (c) SCIG speed, (d) CPL_1 compensation currents, and (e) CPL_1 powers.

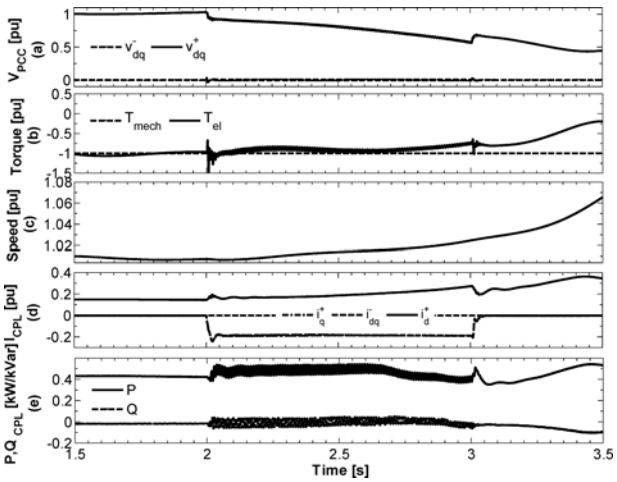

Fig. 8. Simulation results with negative sequence voltage control: (a) PCC voltages, (b) SCIG torque, (c) SCIG speed, (d) CPL_1 compensation currents, and (e) CPL_1 powers.

by

$$\begin{aligned} P_{\mathrm{CPL}} &= v_d^+ i_d^+ + v_d^- i_d^+ + v_q^- i_q^+ \\ Q_{\mathrm{CPL}} &= v_d^+ i_q^+ + v_d^- i_q^+ - v_q^- i_d^+ . \end{aligned} \tag{20}$$

The torque ripples in the SCIG still remain as illustrated by Fig. 7(b) due to the presence of negative sequence voltages in the system.

C. CPLs With Negative Sequence Voltage Control

Fig. 8 illustrates the results when CPLs are controlled to compensate the negative sequence voltage only. The CPL control strategy completely eliminates the negative sequence component of the PCC voltage as shown in Fig. 8(a). CPLs inject the negative sequence component of active and reactive current i_{dq}^- for this purpose as shown in Fig. 8(d). This leads to significant reduction of heavy torque ripples during the fault [see Fig. 8(b)]. As the positive sequence component of the voltage is not compensated, therefore, the rotor keeps on accelerating and

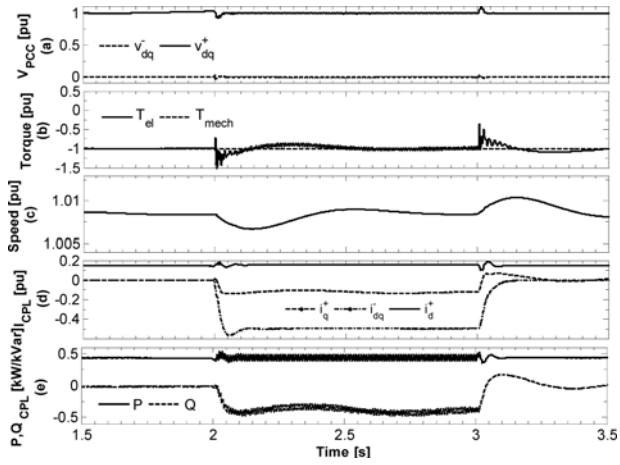

Fig. 9. Simulation results with coordinated positive and negative sequence voltage control: (a) PCC voltages, (b) SCIG torque, (c) SCIG speed, (d) CPL_1 compensation currents, and (e) CPL_1 powers.

SCIG consumes more reactive power from the grid, resulting in a continuous decrease in the positive sequence voltage component and eventually the voltage collapses. The system reaches the mechanical unstable point and cannot return to the rated operating point after the fault. Fig 8(e) shows the oscillating CPL active and reactive powers during the fault. In this case, the active and reactive powers can be represented by

$$\begin{aligned} P_{CPL} &= v_d^+ i_d^+ + v_d^- i_d^- + v_q^- i_q^- + v_d^- i_d^+ + v_d^+ i_d^- \\ Q_{CPL} &= v_d^- i_q^- - v_q^- i_d^- - v_q^- i_d^+ - v_d^+ i_q^- . \end{aligned} \tag{21}$$

During the fault, both the active and reactive powers exhibit second-order harmonics as a result of interaction between the opposite sequence voltage and current components. The input active power oscillates around a constant load demand. The power oscillations under fault condition are higher in this case as confirmed by (21) compared to the previously discussed two cases.

D. CPLs With Coordinated Positive and Negative Sequence Voltage Control

In this case, CPL control is allowed to compensate for both the positive and negative sequence voltage components independently under the same fault conditions. The results are illustrated in Fig. 9. Each CPL injects both the positive and negative sequence of the current for compensation purpose without exceeding its nominal current. The CPL control effectively compensates the positive and negative sequence voltages during the fault. It can also be observed that coordinated voltage control results in the substantial reduction of torque ripples and the acceleration of the rotor during the fault is avoided. SCIG regains the rated operating point during and after the fault. The power relationship is represented by (17) because all the positive and negative sequence voltage and current components are present in this case.

Simulation results enhance the understanding of the operation of SCIG-based wind farm when CPLs are controlled to

provide the positive and negative sequence voltage compensation independently. The positive sequence voltage compensation enhances the torque capability of the SCIG and avoids the acceleration of the rotor, while the negative sequence voltage compensation helps to improve the lifetime of the generator drive train by removing the torque ripples. This is a situation where built-in distribution system resources are able to provide the FRT ancillary service that was earlier supposed to be achieved with a dedicated STATCOM or DFIG-based wind farm arrangements. However, voltage compensation capability is totally dependent on the chosen current rating of the individual CPL. These devices have to be designed for a current rating that must be higher than the active component of current representing their load power requirements.

VI. Incremental Current Rating of the CPL for FRT

This section presents the impact of negative sequence voltage compensation on the total current rating of the CPL. As indicated by (1), the voltage support comes at the cost of reactive current injection under balanced grid faults. The improvement in the voltage profile leads to the reduction of active component of current to keep the input power constant. This is analogous to the previously discussed case of positive sequence voltage compensation under unbalanced grid faults, while the negative sequence voltage still remains in the system. Under this condition, total CPL current I_t^+ can be expressed, such that

$$I_t^+ = \sqrt{(i_d^+)^2 + (i_q^+)^2}. \tag{22}$$

It is supposed in this investigation that CPL is designed to provide the positive sequence voltage compensation through reactive power ancillary service. In order to mitigate the negative sequence effects in the system, the CPLs have to inject the negative sequence current of double grid frequency during the fault. This demands an increment in the total current rating of the each CPL. In this case, the total CPL current $I_{\mathrm{CPL},N}$ can be represented by

$$\begin{aligned} I_{\mathrm{CPL},N} &= \sqrt{(i_d^+)^2 + (i_q^+)^2 + (i_d^-)^2 + (i_q^-)^2} \\ &= \sqrt{(I_t^+)^2 + (I_t^-)^2} \end{aligned} \tag{23}$$

where I_t^- is the total negative sequence current in SRF.

The distribution system model of Fig. 4 is considered with each CPL consuming 450 kW. Single phase to ground fault at the medium voltage bus is simulated to get the different values of voltage sags. Simulations are performed with and without the compensation of negative sequence voltage and the results are presented in Fig. 10. It can be observed that the total CPL current is higher for FRT enhancement of deeper voltage dip. This is due to the increment in the positive and negative sequence compensation currents for FRT enhancement. Before the fault occurs, each CPL is consuming only the active component of positive sequence current corresponding to the load requirements. The value of this current is 0.15 p.u. For a single-phase voltage dip of 70%, the total CPL current increase to 0.37 p.u. This is 150% increment in the total CPL current compared to the prefault value. However, for a higher voltage dip, the positive sequence voltage drops rapidly at the LV bus and CPL has to draw more positive sequence current in accordance with (1) if there is no FRT enhancement provided by CPLs. This also requires an increment in the total CPL current and the system is highly vulnerable to a voltage collapse. Therefore, a demand for an increase in the current rating of the CPL is essential to avoid a complete voltage collapse.

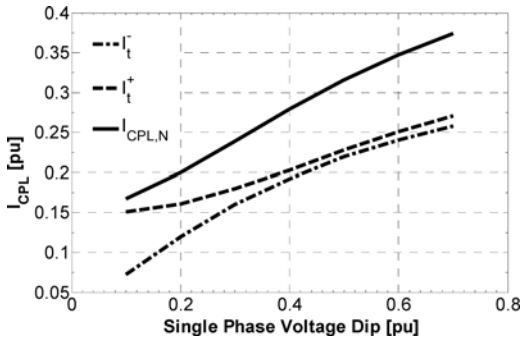

Fig. 10. Incremental current rating of the CPL as a function of single phase to ground fault.

VII. Centralized STATCOM Versus Distributed CPLs

In order to evaluate the extra functionality of each CPL belonging to a group of distributed CPLs for FRT enhancement, a comparison is made with the operation of a centralized STATCOM. A simulation study is performed in order to know the impact of distributed compensation on the total current of each device compared to a STATCOM. The distribution system model used for this purpose is shown in Fig. 4. A comparison between the system with a STATCOM and three noncontrolled CPLs is made with the case of two, three, and four CPLs with FRT capability. Like the previous cases, the total power drawn by the each CPL is 450 kW. Simulations are carried out for different levels of single phase to ground voltage dips at medium voltage bus. The total compensating current I_{COMP} in this case is represented by

$$I_{\mathrm{COMP}} = \sqrt{(i_q^+)^2 + (i_d^-)^2 + (i_q^-)^2}. \tag{24}$$

The amount of total compensating current for FRT enhancement is plotted in Fig. 11 for different fault levels. Each individual CPL injects an amount of current according to the voltage drop at PCC. The voltage drop across each CPL is almost the same, therefore, all the CPLs inject almost equal amount of current for FRT enhancement. It can be observed that the total compensating current by the STATCOM for all the fault levels is higher compared to the total compensating current by a single CPL belonging to a group of two, three, and four distributed CPLs. The higher the number of distributed CPLs in the distribution system, the lower the compensating current injected by individual device. However, the sum of total distributed compensating current for all the studied cases is higher compared to the centralized STATCOM. This is because of the varying distance of the CPLs from PCC. In general, it can be concluded

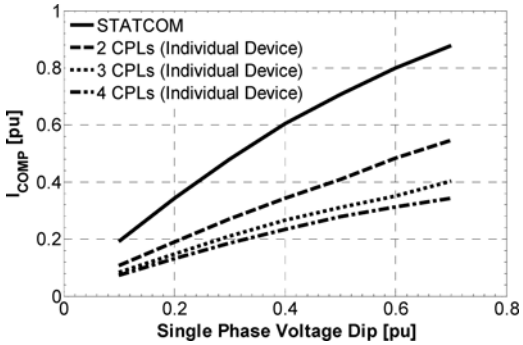

Fig. 11. Total compensating current comparison between STATCOM and distributed CPLs for FRT enhancement.

that the distributed compensation as an ancillary service provided by CPLs is beneficial than centralized compensation and it demands the lower current rating for the individual devices.

VIII. Conclusion

This paper explores the possibility of using distributed CPLs to mitigate the asymmetrical grid faults in a distribution system supplied by SCIG-based wind farm. The proposed system configuration provides an alternative to the conventional STATCOM and DFIG wind turbine by effectively controlling the installed resources at the distribution level. A detailed simulation analysis is carried out to understand the voltage control performed by distributed CPLs and the resulting operation of the SCIG under unbalanced grid fault. A DSOGI-PLL is employed in the control strategy of each CPL for the precise extraction of positive and negative sequence voltage components. A CPL control structure is proposed to achieve the independent compensation of positive and negative sequence of the voltage. The priority has been assigned to the positive sequence voltage control for the maximum FRT enhancement of the SCIG-based wind farm. The positive sequence voltage compensation avoids the acceleration of the rotor and prevents the voltage collapse under severe grid side faults. The negative sequence voltage control is performed to remove the torque oscillation in the SCIG during the asymmetrical fault and it improves the lifetime of the drive train. The incremental current rating of the semiconductor switches of the CPLs is studied and it is observed that the deeper the voltage drop, the higher the CPL current rating required for FRT enhancement. The total compensating current injected by the individual CPL belonging to a group of distributed CPLs is compared with the total compensating current by a centralized STATCOM. It is found that the each distributed CPL injects less current for FRT enhancement compared to one centralized STATCOM.

References

[1] A. Camacho, M. Castilla, J. Miret, J. C. Vasquez, and E. Alarcon-Gallo, "Flexible voltage support control for three-phase distributed generation inverters under grid fault," *IEEE Trans. Ind. Electron.*, vol. 60, no. 4, pp. 1429–1441, Apr. 2013.

[2] M. Goyal and R. Gupta, "Power flow control in distributed microgrid with wind energy system," in *Proc. Students Conf. Eng. Syst.*, 2012, pp. 1–5.

[3] EWEA, "Large scale integration of wind energy in the European power supply: Analysis, issues and recommendations," European Wind Energy Assoc., Tech. Rep., 2005.

[4] I. Erlich, W. Winter, and A. Dittrich, "Advanced grid requirements for the integration of wind turbines into the German transmission system," in *Proc. IEEE Power Eng. Soc. General Meet.*, 2006, p. 7.

[5] P. Rodriguez, A. Luna, G. Medeiros, R. Tedorescu, and F. Blaabjerg, "Control of STATCOM in wind power plants based on induction generators during asymmetrical grid faults," in *Proc. Int. Power Electron. Conf.*, 2010, pp. 2066–2073.

[6] L. Chia-Tse, H. Che-Wei, and C. Po-Tai, "A low-voltage ride-through technique for grid-connected converters of distributed energy resources," *IEEE Trans. Ind. Appl.*, vol. 47, no. 4, pp. 1821–1832, Jul./Aug. 2011.

[7] C. Shih-Feng, L. Chia-Tse, C. Po-Tai, and F. Blaabjerg, "A reactive current injection technique for renewable energy converters in low voltage ride-through operations," in *Proc. IEEE Power Energy Soc. General Meet.*, 2011, pp. 1–7.

[8] O. A. Giddani, G. P. Adam, O. Anaya-Lara, G. Burt, and K. L. Lo, "Control strategies of VSC-HVDC transmission system for wind power integration to meet GB grid code requirements," in *Proc. Int. Symp. Power Electron. Electr. Drives Autom. Motion*, 2010, pp. 385–390.

[9] Energinet, "Regulation TF 3.2.6 Wind Turbines Connected to Grids With Voltages Below 100 kV," Denmark, May 19, 2010.

[10] Energinet, "Regulation TF 3.2.5 Wind Turbines Connected to Grids With Voltages Above 100 kV," Denmark, Dec. 3, 2010.

[11] H. Chaal and M. Jovanovic, "Toward a generic torque and reactive power controller for doubly fed machines," *IEEE Trans. Power Electron.*, vol. 27, no. 1, pp. 113–121, Jan. 2012.

[12] H. Xu, J. Hu, and Y. He, "Operation of wind-turbine-driven DFIG systems under distorted grid voltage conditions: Analysis and experimental validations," *IEEE Trans. Power Electron.*, vol. 27, no. 5, pp. 2354–2366, May 2012.

[13] J. Yao, H. Li, Z. Chen, X. Xia, X. Chen, Q. Li, and Y. Liao, "Enhanced control of a DFIG-based wind-power generation system with series grid-side converter under unbalanced grid voltage conditions," *IEEE Trans. Power Electron.*, vol. 28, no. 7, pp. 3167–3181, Jul. 2013.

[14] Y. Wang, L. Xu, and W. B. W , "Compensation of network voltage unbalance using doubly fed induction generator-based wind farms," *Renewable Power Gen., IET*, vol. 1, pp. 12–22, 2009.

[15] S. Deshmukh, B. Natarajan, and A. Pahwa, "Voltage/VAR control in distribution networks via reactive power injection through distributed generators," *IEEE Trans. Smart Grid*, vol. 3, no. 3, pp. 1226–1234, Sep. 2012.

[16] C. Wessels, S. Grunau, and F. Fuchs, "Current injection targets for a statcom under unbalanced grid voltage condition and the impact on the PCC voltage," in *Proc. IEEE Energy Convers. Congr. Expo.*, Apr. 2011.

[17] P. Rodriguez, G. Medeiros, A. Luna, M. C. Cavalcanti, and R. Teodorescu, "Safe current injection strategies for a STATCOM under asymmetrical grid faults," in *Proc. IEEE Energy Convers. Congr. Expo.*, 2010, pp. 3929–3935.

[18] M. Molinas, S. Jon Are, and T. Undeland, "Low voltage ride through of wind farms with cage generators: STATCOM versus SVC," *IEEE Trans. Power Electron.*, vol. 23, no. 3, pp. 1104–1117, May 2008.

[19] J. A. Suul, M. Molinas, and T. Undeland, "STATCOM-based indirect torque control of induction machines during voltage recovery after grid faults," *IEEE Trans. Power Electron.*, vol. 25, no. 5, pp. 1240–1250, May 2010.

[20] M. Belkhayat, R. Cooley, and A. Witulski, "Large signal stability criteria for distributed systems with constant power loads," in *Proc. Record. IEEE 26th Annu. Power Electron. Spec. Conf.*, 1995, vol. 2, pp. 1333–1338.

[21] M. Belkhayat, "Stability criteria for AC power systems with regulated loads," Thesis for the Degree of Doctor of Philosophy, Purdue Univ., West Lafayette, IN, USA, Dec. 1997.

[22] W. Du, J. Zhang, Y. Zhang, and Z. Qian, "Stability criterion for cascaded system with constant power load," *IEEE Trans. Power Electron.*, vol. 28, no. 4, pp. 1843–1851, Apr. 2013.

[23] D. Marx, P. Magne, B. Nahid-Mobarakeh, S. Pierfederici, and B. Davat, "Large signal stability analysis tools in DC power systems with constant power loads and variable power loads—A review," *IEEE Trans. Power Electron.*, vol. 27, no. 4, pp. 1773–1787, Apr. 2012.

[24] A. Emadi, "Modeling of power electronic loads in AC distribution systems using the generalized State-space averaging method," *IEEE Trans. Ind. Electron.*, vol. 51, no. 5, pp. 992–1000, Oct. 2004.

[25] A. Emadi, A. Khaligh, C. H. Rivetta, and G. A. Williamson, "Constant power loads and negative impedance instability in automotive systems: definition, modeling, stability, and control of power electronic converters and motor drives," *IEEE Trans. Veh. Technol.*, vol. 55, no. 4, pp. 1112–1125, Jul. 2006.
[26] A. Khaligh, A. M. Rahimi, and A. Emadi, "Modified pulse-adjustment technique to control DC/DC converters driving variable constant-power loads," *IEEE Trans. Ind. Electron.*, vol. 55, no. 3, pp. 1133–1146, Mar. 2008.
[27] M. Molinas and J. Kondoh, "Power electronic loads as providers of reactive power ancillary service to the grid: Analytical and experimental study," in *Proc. Eur. Conf. Power Electron. Appl.*, Barcelona, Spain, 2009, pp. 1–10.
[28] P. J. M. Heskes, J. M. A. Myrzik, and W. L. Kling, "Power electronic loads with negative differential impedance in a low voltage distribution system," in *Proc. 20th Int. Conf. Electricity Distrib.*, Prague, 2009.
[29] N. Jelani and M. Molinas, "Mitigation of asymmetrical grid faults in induction generator-based wind turbines using constant power load," *Energies, MDPI*, vol. 6, pp. 1700–1717, 2013.
[30] M. Molinas, D. Moltoni, G. Fascendini, J. A. Suul, and T. Undeland, "Constant power loads in AC distribution systems: An investigation of stability," in *Proc. IEEE Int. Symp. Ind. Electron.*, 2008, pp. 1531–1536.
[31] G. M. S. Azevedo, P. Rodriguez, M. C. Cavalcanti, G. Vazquez, and F. A. S. Neves, "New control strategy to allow the photovoltaic systems operation under grid faults," in *Proc. Power Electron. Conf.*, 2009, pp. 196–201.
[32] A. B. Jusoh, "The instability effect of constant power loads," in *Proc. Nat. Power Energy Conf.*, 2004, Malaysia, pp. 175–179.
[33] N. Jelani and M. Molinas, "Stability investigation of control system for power electronic converter acting as load interface in AC distribution system," in *Proc. IEEE Int. Symp. Ind. Electron.*, 2011, pp. 408–413.
[34] J. A. Suul, A. Luna, P. Rodriguez, and T. Undeland, "Virtual-flux-based voltage-sensor-less power control for unbalanced grid conditions," *IEEE Trans. Power Electron.*, vol. 27, no. 9, pp. 4071–4087, Sep. 2012.
[35] P. Rodriguez, A. Luna, R. S. Muñoz-Aguilar, I. Etxeberria-Otadui, R. Teodorescu, and F. Blaabjerg, "A stationary reference frame grid synchronization system for three-phase grid-connected power converters under adverse grid conditions," *IEEE Trans. Power Electron.*, vol. 27, no. 1, pp. 99–112, Jan. 2012.
[36] P. Rodriguez, A. Luna, M. Ciobotaru, R. Teodorescu, and F. Blaabjerg, "Advanced grid synchronization system for power converters under unbalanced and distorted operating conditions," in *Proc. IEEE 32nd Annu. Conf. Ind. Electron.*, 2006, pp. 5173–5178.
[37] P. Rodriguez, R. Teodorescu, I. Candela, A. V. Timbus, M. Liserre, and F. Blaabjerg, "New positive-sequence voltage detector for grid synchronization of power converters under faulty grid conditions," in *Proc. IEEE 37th Power Electron. Spec. Conf.*, 2006, pp. 1–7.
[38] M. Ciobotaru, R. Teodorescu, and F. Blaabjerg, "A new single-phase PLL structure based on second order generalized integrator," in *Proc. IEEE 37th Power Electron. Spec. Conf.*, 2006, pp. 1–6.
[39] P. Tenti, A. Costabeber, P. Mattavelli, and D. Trombetti, "Distribution loss minimization by token ring control of power electronic interfaces in residential microgrids," *IEEE Trans. Ind. Electron.*, vol. 59, no. 10, pp. 3817–3826, Oct. 2012.
[40] O. Noureldeen, "Low voltage ride through strategies for SCIG wind turbines interconnected grid," *Int. J. Electr. Comput. Sci.*, vol. 11, no. 2.
[41] O. Anaya-Lara, N. Jenkins, J. Ekanayake, P. Cartwright, and M. Hughes, *Wind Energy Generation: Modelling and Control*. New York, NY, USA: Wiley, 2009.

Nadeem Jelani (M'10) was born in Pakistan in 1981. He received the B.Sc. degree in electrical engineering from the University of Engineering and Technology, Peshawar, Pakistan, in 2004 and the M.Sc. degree in electric power engineering from the Norwegian University of Science and Technology, Trondheim, Norway, in 2010, where he is currently working toward the Ph.D. degree in the Department of Electric Power Engineering.

His research interests include control of power electronics converters in power systems, smartgrids and for renewable energy applications.

Marta Molinas (M'94) received the Diploma degree in electromechanical engineering from the National University of Asuncion, San Lorenzo, Paraguay, in 1992, the M.Sc. degree from the University of the Ryukyus, Nishihara, Japan, in 1997, and the Dr.Eng. degree from the Tokyo Institute of Technology, Meguro, Japan, in 2000.

In 1998, she was a Guest Researcher with the University of Padua, Italy. From 2004 to 2007, she was a Postdoctoral Researcher with the Norwegian University of Science and Technology, Trondheim, Norway, where she has been a Professor since 2008. From 2008 to 2009, she was a JSPS Research Fellow with the Energy Technology Research Institute, National Institute of Advanced Industrial Science and Technology, Tsukuba, Japan. Her research interests include wind/wave energy conversion systems and power electronics and electrical machines in distributed energy systems.

Dr. Molinas is an Active Reviewer for the IEEE TRANSACTIONS ON INDUSTRIAL ELECTRONICS and the IEEE TRANSACTIONS ON POWER ELECTRONICS. She is an Associate Editor of the IEEE TRANSACTIONS ON POWER ELECTRONICS. She was an Administrative Committee Member of the IEEE Power Electronics Society in 2009–2011.